

# Off-axis digital holography with multiplexed volume Bragg gratings

Leo Puyo,<sup>1</sup> Jean-Pierre Huignard,<sup>1</sup> and Michael Atlan<sup>1</sup>

<sup>1</sup>Centre National de la Recherche Scientifique (CNRS) UMR 7587,

Institut Langevin. Paris Sciences et Lettres (PSL) Research University. Fondation Pierre-Gilles de Gennes,

Institut National de la Santé et de la Recherche Médicale (INSERM) U 979, Université Pierre et Marie Curie (UPMC),

Université Paris 7. École Supérieure de Physique et de Chimie Industrielles ESPCI Paris - 1 rue Jussieu. 75005 Paris. France

(Dated: April 27, 2018)

We report on an optical imaging design based on common-path off-axis digital holography, using a multiplexed volume Bragg grating. In the reported method, a reference optical wave is made by deflection and spatial filtering through a volume Bragg grating. This design has several advantages including simplicity, stability and robustness against misalignment.

## INTRODUCTION

The success of the Zernike phase-contrast microscope [1] has led to a number of subsequent phase-imaging methods, including Nomarski differential interference contrast microscopy [2] and Hoffman modulation contrast microscopy [3]. Those phase-contrast methods merge brightness and phase information in the recorded image. Later on, quantitative phase shifts of an object wave beating against a reference wave were measured by phase-contrast digital holography [4]. In digital holography, this phase is derived from the measurement of spatiotemporal variations in intensity of the interference pattern, digitized by a sensor array, and digital image rendering by wave propagation computation. Since then, holographic phase microscopy has emerged as a powerful imaging technique for probing quantitatively refractive index changes in transparent samples [5]. Optical phase microscopy techniques based on interferometric recordings and computational image rendering have become widely available since then [6–8], and have opened the way to tomographic phase microscopy [9–13].

On-axis interferometry, the original Gabor configuration for hologram recording [14], has the advantage of being easily realized experimentally, but lacks of sensitivity [15] and might prevent accurate phase reconstructions [16, 17]. In contrast, in off-axis recording configuration [18], the average propagation directions of the reference and the object optical waves, interfering in the sensor plane, are slightly tilted. The spatial spectrum of the hologram is shifted by a quantity which scales as the average tilt angle. This tilt permits the separation and discrimination of self-beating and cross-beating interferometric contributions of the object and the reference optical fields; spurious interferometric contributions can be filtered-off [19], and phase imaging can be performed straightforwardly [4]. In addition, the optical paths of light impinging on the sensor can have either both probed the sample in common-path configurations or taken different pathways in separate

arms configurations. Common-path interferometry configurations, for which both waves travel the same pathways (quasi-)through the sample [20–23] prevent phase noise from pathlength fluctuations of the reference beam decorrelated from the object beam, mode hops, and increase the overall stability of the interferogram. A significant improvement of off-axis interferometry with short coherence radiation was achieved by the use of diffraction gratings to tilt the coherence plane with respect to the direction of propagation of the reference wave, so that cross-interference patterns cover all the detector array [24–30].

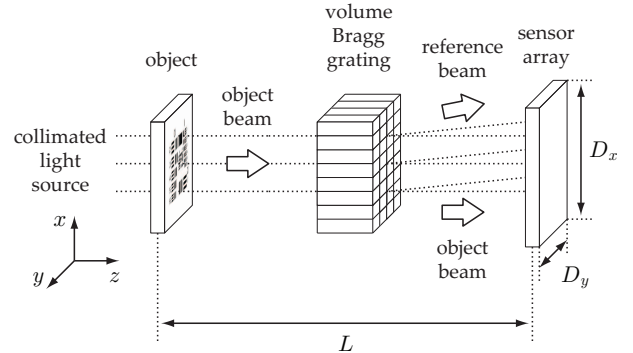


FIG. 1: Sketch of the experimental setup. A phase object is illuminated in transmission configuration, and the output field is partly deflected and filtered by a multiplexed volume Bragg grating to create an off-axis reference beam interfering with the object beam on a sensor array.

We propose here a new simple off-axis digital holographic microscopic scheme inspired by 1- point-diffraction interferometry approaches [31–33], and their refinements [34–37], in which a reference optical wave is formed by spatial filtering of a replica of the object wave. 2- off-axis implementations of phase-contrast digital holographic microscopy [4, 21, 38–40], 3- lateral shearing interferometry [41, 42], 4- the angular filtering properties of volume Bragg gratings [43, 44], recorded in the volume of doped glasses with photothermorefractive processes [45], and 5- an implementation of volume Bragg gratings for

obtaining digital holograms in a self-reference configuration in a conventional microscope [46]. In the reported design, a reference optical wave, suitable for off-axis holographic interferometry is made by deflection through a volume Bragg grating.

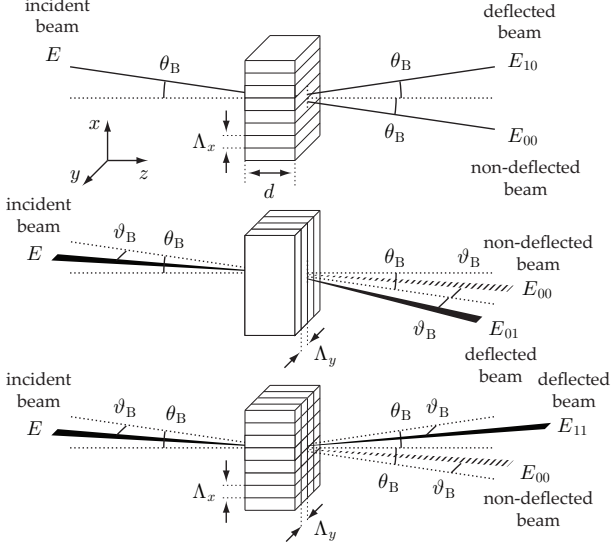


FIG. 2: Deflection and filtering of the optical field  $E$  by volume Bragg gratings. The light deflected by  $2\theta_B \sim \lambda/\Lambda_x$  and/or  $2\vartheta_B \sim \lambda/\Lambda_y$  is filtered spatially. The  $k_x$  content of the output field  $E_{10}$  is lowpass filtered with an angular selectivity  $\Delta\theta_1 \sim n_0\Lambda_x/d$ . The  $k_y$  content of the output field  $E_{01}$  is lowpass filtered with an angular selectivity  $\Delta\vartheta_1 \sim n_0\Lambda_y/d$ . The  $(k_x, k_y)$  content of the output field  $E_{11}$  is lowpass filtered with an angular selectivity  $(\Delta\theta_1, \Delta\vartheta_1)$ . The non-deflected beam  $E_{00}$  has an angular bandwidth  $(\Delta\theta_0, \Delta\vartheta_0)$ ; it is not filtered.

## EXPERIMENTAL SETUP

### Optical configuration

In the experimental setup sketched in Fig. 1, a microscopic object is illuminated in transmission by a laser (Crystalaser DL660-100, wavelength  $\lambda \sim 660$  nm, coherence length 0.3 mm). The transmitted object field can be magnified by a microscope objective or merely occulted partially by a pupil, before passing through a diffractive optical element, and impinges on the sensor array of a camera (Ximea MQ042MG-CM, array size:  $2048 \times 2048$  pixels, pitch:  $5.5 \mu\text{m}$ ). In the absence of microscope objective, the angular bandwidth  $(\Delta\theta_0, \Delta\vartheta_0)$  of the object field  $E_{00}$  impinging on the sensor array is limited by the aperture stop of the system, which can either be a pupil introduced between the object and the sensor, or the sensor itself. In the former case,  $\Delta\theta_0 \approx a_x/l$ , and  $\Delta\vartheta_0 \approx a_y/l$ , where  $a_x$  and  $a_y$  are the aperture dimensions in the  $x$  and  $y$  directions, and  $l$  is the object-to-pupil distance.

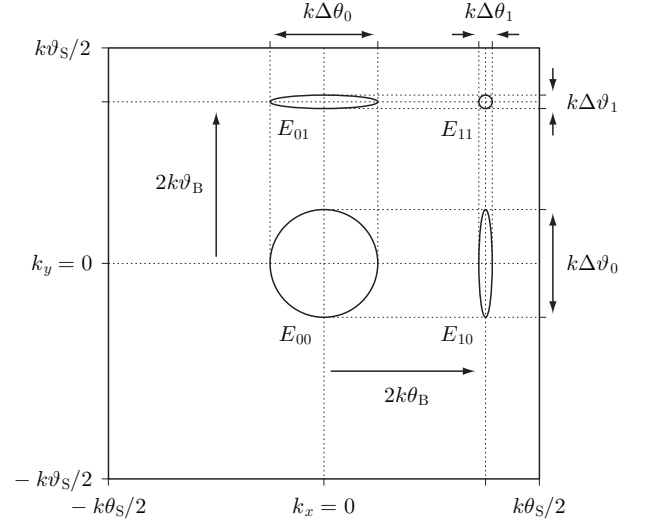


FIG. 3: Angular wavevector  $(k_x, k_y)$  representation of the transmitted beams, in the Fourier plane of the exit face of the volume Bragg gratings. The angular bandwidth  $(\Delta\theta_0, \Delta\vartheta_0)$  of non-deflected optical field  $E_{00}$  is limited by the pupil and measured between the marginal rays touching its edges. The boundaries of the angular field of the detection are the Nyquist angles  $(\pm\theta_S/2, \pm\vartheta_S/2)$ , and its extent is the angular acceptance of the coherent detection  $(\theta_S, \vartheta_S)$ . The shift and angular bandwidth of the fields  $E_{10}$  and  $E_{01}$  deflected by the first and second regular gratings of Fig. 2 are represented. Those fields are allowed to pass when one of the Bragg conditions is not met with the multiplexed grating (Fig. 2, bottom) but their presence is cancelled when both Bragg conditions are fulfilled. In that case, the reference field  $E_{11}$  is deflected by  $(2\theta_B, 2\vartheta_B)$  with respect to the object beam, and low-pass filtered within the angular width  $(\Delta\theta_1, \Delta\vartheta_1)$  of the Bragg diffraction efficiency function [47].

In the latter case,  $\Delta\theta_0 \approx D_x/L$ , and  $\Delta\vartheta_0 \approx D_y/L$ , where  $D_x$  and  $D_y$  are the sensor dimensions in the  $x$  and  $y$  directions, and  $L$  is the object-to-sensor distance. If a microscope objective is present, the angular bandwidth of the object field is limited by the numerical aperture NA of the objective :  $\Delta\theta_0 = \Delta\vartheta_0 = 2 \arcsin(\text{NA})$ . A usual method to engineer a reference optical wave suitable for off-axis holographic interferometry from the object wave itself consists in reducing the spatial frequency content of the latter by low-pass filtering of the transverse projections of the transmitted angular wavenumbers  $(k_x, k_y)$  with a pinhole [31, 34, 48, 49], or by defocus by curved mirrors [50], a spatial light modulator [51], or lenses [22, 52, 53].

### Angular filtering by a multiplexed Bragg grating

In our novel approach, a reference optical wave is made by deflection at the Bragg angle through a multiplexed grating. For this purpose, a transmission vol-

ume Bragg grating created by double interferometric exposure in a photothermorefractive glass was realized by OptiGrate [45, 54]. It displays a periodic change in the refractive index  $n$  of the form

$$n(x, y) = n_0 + n_1 \sin\left(\frac{2\pi x}{\Lambda_x}\right) + n_2 \sin\left(\frac{2\pi y}{\Lambda_y}\right) \quad (1)$$

where  $n_0 = 1.498$  is the average refractive index of the glass, and  $n_1 = n_2 \sim 1.4 \times 10^{-5}$  is its modulation depth in each transverse direction,  $x$ , and  $y$ . It acts as a superposition of two perpendicular phase gratings, sketched in Fig. 2. The thickness of the multiplexed grating is  $d = 8.9$  mm. The grating periods are  $\Lambda_x = 18.9 \mu\text{m}$ , and  $\Lambda_y = 18.3 \mu\text{m}$ . The relative diffraction efficiency (for plane waves, when the Bragg condition is fulfilled) of the horizontal and the vertical grating are  $|E_{01}|^2/(|E_{00}|^2 + |E_{01}|^2) = 0.56$ , and  $|E_{10}|^2/(|E_{00}|^2 + |E_{10}|^2) = 0.55$ .

The Bragg condition defines the angle of deflection of a given input beam. For an unslanted grating, in the configuration sketched in Fig. 2, we have

$$2 \sin(\theta_B) = \frac{\lambda}{\Lambda_x} \quad \text{and} \quad 2 \sin(\vartheta_B) = \frac{\lambda}{\Lambda_y} \quad (2)$$

where  $\Lambda_x$  and  $\Lambda_y$  are the grating periods. The spatial filtering properties of transmission volume Bragg gratings constrain the degree of collimation of the input beam allowed to be deflected by twice the Bragg angles. The angular efficiency, defined by the grating angular diffraction efficiency [47] sets the angular support  $\Delta\theta_1$  and  $\Delta\vartheta_1$  of the deflected fields in  $x$  and  $y$  respectively, given by

$$\Delta\theta_1 \approx n_0 \frac{\Lambda_x}{d} \quad \text{and} \quad \Delta\vartheta_1 \approx n_0 \frac{\Lambda_y}{d} \quad (3)$$

where  $n_0$  is the average refractive index of the material, and  $d$  is the thickness of the grating [43, 44]. When both Bragg conditions are fulfilled for the multiplexed Bragg grating (Fig. 2(c)), the input angles of the object beam are  $\theta_B$  and  $\vartheta_B$ , the deviation angles of the first diffraction orders are predicted by Bragg's law (Eq. 2), and only low spatial frequencies  $k_x \in [-k\Delta\theta_1/2, k\Delta\theta_1/2]$  and  $k_y \in [-k\Delta\vartheta_1/2, k\Delta\vartheta_1/2]$  are allowed to pass in the deflected beam, yet the spatial frequency content of the non-deflected beam is unaffected by transmission through the grating. The angular representation of the corresponding optical fields,  $E_{00}$  and  $E_{11}$  respectively, are reported in Fig 3. The shift and angular bandwidth of the fields  $E_{10}$  and  $E_{01}$  deflected by the first and second regular gratings of Fig. 2 are also reported in Fig 3. The spatial filtering property is the key to the realization of the tilted reference wave in common-path transmission interferometric configuration. With the chosen grating thickness of  $d \simeq 9$  mm, this angular filter of acceptance  $\Delta\theta_1 = \Delta\vartheta_1 \simeq 3.3$  mrad is equivalent to the angular selectivity  $\sim D/f \simeq 3.3$  mrad of a pinhole of diameter

$D = 330 \mu\text{m}$ , set in the focal plane of a converging lens of focal length  $f = 10$  cm in a point-diffraction interferometer [31–33]. The choice of grating periods  $\Lambda_x$  and  $\Lambda_y$  is dictated by the NyquistShannon sampling theorem: the deflection angles of the propagation directions of  $E_{11}$  and  $E_{00}$  have to satisfy  $2\theta_B \in [-\theta_S/2, \theta_S/2]$ , and  $2\vartheta_B \in [-\vartheta_S/2, \vartheta_S/2]$  where

$$\theta_S \approx \frac{\lambda}{d_x} \quad \text{and} \quad \vartheta_S \approx \frac{\lambda}{d_y} \quad (4)$$

are the angular acceptances of the coherent detection on an array detector [55], with pixels spaced by  $d_x$  and  $d_y$  along  $x$  and  $y$ , respectively. The pixel pitches of the camera used in the experiments are  $d_x = d_y = 5.5 \mu\text{m}$ . Eq. 2, Eq. 3, and Eq 4 are valid for small input and output angles, in the paraxial approximation [47]. In order to achieve typical off-axis detunings between the object and the reference waves, deflection angles have to be about one half of the Nyquist angles  $\theta_S/2$  and  $\vartheta_S/2$  typically, and hence satisfy the relations  $2\theta_B \sim \theta_S/4$ , and  $2\vartheta_B \sim \vartheta_S/4$ , which impose grating periods of  $\Lambda_x \sim 4d_x$  and  $\Lambda_y \sim 4d_y$ .

#### Experimental validation of angular filtering and deflection by a multiplexed Bragg grating

To illustrate the spatial filtering properties of the Bragg orders, we placed a converging lens between the grating and the sensor array to form the image of the resolution target in the detection plane. In Fig. 4(a), the Bragg condition is not met for any beam direction, only the non-deflected beam (field  $E_{00}$ ) is transmitted. The angular bandwidth of the object field  $E_{00}$  is completely transmitted through the grating, and spatial frequencies are bounded by  $(k\Delta\theta_0, k\Delta\vartheta_0)$ , as sketched in Fig. 3. In Fig. 4(b), the Bragg condition is met only for  $\theta$  tilt ( $x$  direction); the non-deflected beam (field  $E_{00}$ ) and the beam deflected by  $2\theta_B$  (field  $E_{10}$ ) are transmitted. The angular bandwidth of the deflected field  $E_{10}$  is reduced. Its spatial frequencies are bounded by  $(k\Delta\theta_1, k\Delta\vartheta_0)$ , as sketched in Fig. 3. Hence, horizontal bars of the deflected image are no longer visible. In Fig. 4(c), the Bragg condition is met only for  $\vartheta$  tilt ( $y$  direction); the non-deflected beam (field  $E_{00}$ ) and the beam deflected by  $2\vartheta_B$  (field  $E_{01}$ ) are transmitted. The angular bandwidth of the deflected field  $E_{01}$  is reduced. Its spatial frequencies are bounded by  $(k\Delta\theta_0, k\Delta\vartheta_1)$ , as sketched in Fig. 3. Hence, vertical bars of the deflected image are no longer visible. When the Bragg condition is fulfilled for both directions, the non-deflected beam  $E_{00}$ , the deflected and spatially-filtered beams  $E_{10}$  and  $E_{01}$  are transmitted, as reported in Fig. 4(d). A fourth beam, deflected both in  $\theta$  and  $\vartheta$  by  $2\theta_B$  and  $2\vartheta_B$  respectively is transmitted (field  $E_{11}$ ). The angular bandwidth of the deflected field  $E_{11}$  is reduced. Its spatial frequencies are bounded by  $(k\Delta\theta_1, k\Delta\vartheta_1)$ , as

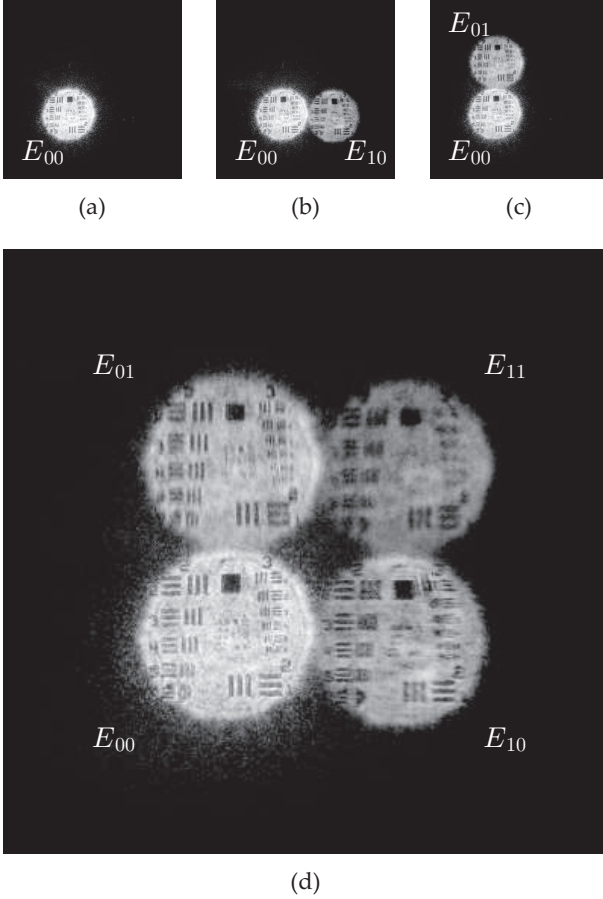


FIG. 4: Experimental images of the target recorded for different tilt angles of the thick Bragg grating, obtained with a physical lens. Bragg conditions (Eqs.2) not satisfied (a), satisfied only for  $\theta$  (b), satisfied only for  $\vartheta$  (c), satisfied for both  $\theta$  and  $\vartheta$  (d).

sketched in Fig. 3. Hence, both horizontal and vertical bars of the deflected image are no longer visible.

## OFF-AXIS HOLOGRAM RECONSTRUCTION

### Fresnel transformation

Holograms were reconstructed by Fresnel transformation [56–63]; in practice, we used the software Holovibes [64] for real-time hologram rendering, which performed image rendering of complex-valued holograms  $H(x, y, t)$  from the stream of rescaled interferograms  $I(x, y, t)$

$$H(x, y, t) = \frac{i}{\lambda z} \exp(-ikz) \iint I(x', y', t) \times \exp\left[\frac{-i\pi}{\lambda z} ((x - x')^2 + (y - y')^2)\right] dx' dy' \quad (5)$$

The parameter  $z$  is the reconstruction distance for which the image of the target appears on the magnitude of the hologram  $|H|$ . The interferometric contributions in the interferogram plane that create fringe sets (Fig. 5(a), and Fig. 5(b)) are separated in the Fourier reciprocal plane (Fig. 5(c)) and the hologram reconstruction plane (Fig. 5(e)).

### Amplitude imaging

In order to record holographic interferograms, we removed the lens between the grating and the sensor array, and we increased the aperture stop of the system to widen the lateral extension of the deflected fields, and make the four contributions interfere in an overlapping region covering most of the sensor area, as shown in the experimental interferogram displayed in Fig. 5(a). A zoomed view in the region of interest depicted by the box, showing the juxtaposition of horizontal and vertical fringes, is reported in Fig. 5(b). When the Bragg conditions are fulfilled for both directions, angular spectra of  $E_{10}$ ,  $E_{01}$ , and  $E_{11}$  are filtered by the Bragg grating angular selectivity, as sketched in Fig. 3. The total transmitted field is the sum of four components forming an interferogram on the sensor array  $I = |E_t|^2$ , where

$$E_t = E_{00} + E_{10} + E_{01} + E_{11} \quad (6)$$

Each set of fringes corresponds to the interference between couples of field components, except self-beating contributions. The reconstructed hologram  $H$  by linear Fresnel transformation (Eq. 5) shifts those contributions according to this fringe structure. The spatial Fourier transform  $\mathcal{F}\{I\}$  of the interferogram  $I$  displayed in Fig. 5(a) takes the form

$$\mathcal{F}\{I\} = E_t * E_t^* \quad (7)$$

where  $*$  is the spatial convolution product. For the sake of notation simplicity, the fields  $E$  either refer to distributions in the sensor plane, or at the exit face of the volume Bragg grating, or their reciprocal planes. The magnitude  $|\mathcal{F}\{I\}|$  is displayed in logarithmic scale in Fig. 5(c), on which one can see nine diffraction locations of the 16 interferometric terms. A sketch of the 16 interference terms locations in a reciprocal plane of the interferogram is reported in Fig. 6.

Among the 16 interferometric terms of  $\mathcal{F}\{I\}$ , the term  $E_{00} * E_{11}^*$  highlighted in Fig. 5(e), and displayed in Fig. 5(d), and its complex conjugate  $E_{00}^* * E_{11}$  are shifted in opposite corners of the reconstructed hologram, and used as off-axis holograms. These contributions are the result of the interference between the transmitted field  $E_{00}$ , and the field of reduced angular support in both directions  $(x, y)$   $E_{11}$  which acts as a flattened reference



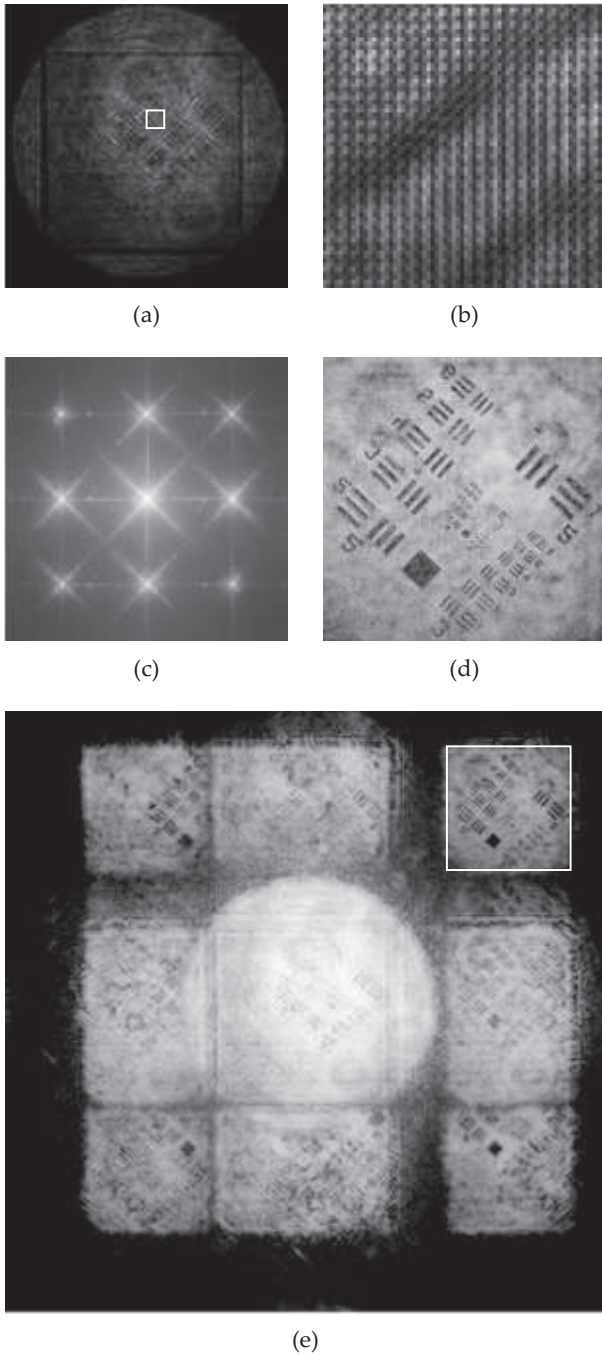


FIG. 5: Amplitude contrast target. (a) Recorded interferogram  $I$ , where the shadow delimiting the edges of the diffraction grating is cast. (b) Magnified view of the fringes in the highlighted region in (a). (c) Amplitude distribution in the Fourier plane  $|\mathcal{F}\{I\}|$  (log. scale). (d) Magnified view of the off-axis area of the magnitude of the hologram  $|H|$  displayed in (e). Amplitude distribution of the Fresnel transform of the interferogram (a), at the distance 0.216 m (e).

wave. In the remaining corners, the beating contributions  $E_{10} * E_{01}^*$  and  $E_{10}^* * E_{01}$  are present. These terms are the result of the beat between transmitted and partly

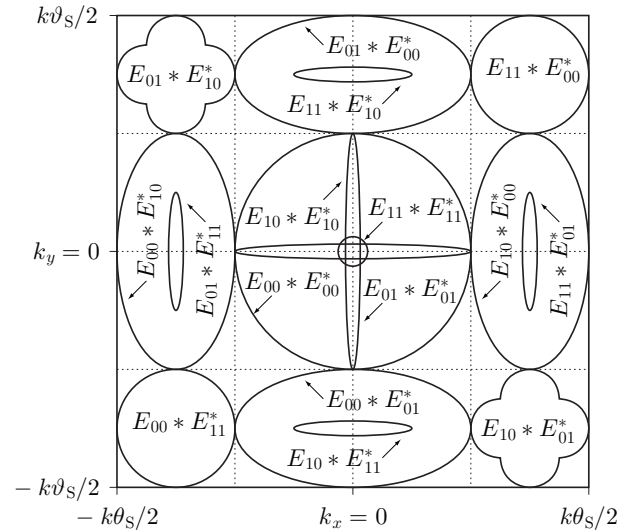


FIG. 6: Sketch of the 16 interference terms locations in the Fourier plane of the interferogram.

filtered fields in the horizontal and vertical directions. In the four sides, the beating contributions  $E_{10} * E_{01}^*$  and  $E_{10}^* * E_{01}$  are present. These terms are the result of the beat between transmitted and partly filtered fields in the horizontal and vertical directions.

### Phase imaging

In order to obtain phase images, holograms were processed to remove artifacts generated by the off-axis configuration [65] and the phase curvature [66] of the reference wave. The interferometric order  $E_{00} * E_{11}^*$  was selected and re-centered in the Fourier space while the rest of the Fourier components were cropped out [4, 65]. These operations allowed for the removal of signal corresponding to other interferometric contribution and also of the off-axis phase tilt. A Fresnel transformation (Eq. 5) was carried out onto the interferograms acquired in the presence [Fig. 7(a)] and absence [Fig. 7(b)] of target. The phase image reported in Fig. 7(g) is the difference between the phase of the reconstructed holograms acquired with [Fig. 7(e)] and without [Fig. 7(f)] target. The accuracy of the phase measurement might be hindered by a not perfectly flat reference wave in the reported results.

### CONCLUSIONS

In conclusion, the reported off-axis common-path holographic interferometer design performs spatial filtering with a multiplexed volume Bragg grating, which makes it suited to the detection of optical absorption and index variations. The described interferometer is lensless, and

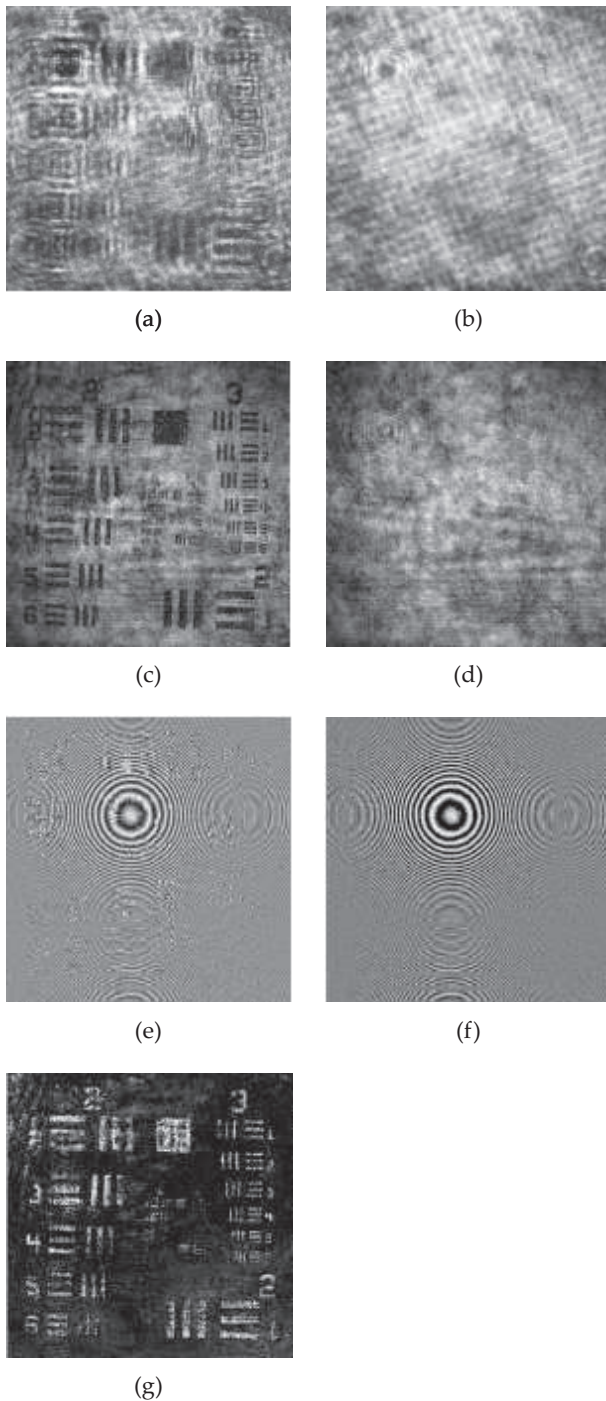


FIG. 7: Image rendering process. Central region of the interferogram acquired, with (a) and without target (b). Amplitude of the holograms reconstructed in the object plane, with (c) and without target (d). Phase of the holograms reconstructed in the object plane, with (e) and without target (f). (g) Difference of the phase holograms (e) and (f).

may be adapted to microscopic imaging. Lateral resolution, robustness against vibration and aberration, spatiotemporal coherence requirements of the radiation and accuracy of phase imaging might be further investigated.

The reported results made use of one thick grating; alternatively, the use of two thinner multiplexed gratings could result in the same deflection and filtering properties [67].

### Funding

This work was supported by the Investments for the Future program (LabEx WIFI: ANR-10-LABX-24, ANR-10-IDEX-0001-02 PSL\*), and European Research Council (ERC Synergy HELMHOLTZ, #610110).

- 
- [1] Frits Zernike. Phase contrast, a new method for the microscopic observation of transparent objects. *Physica*, 9(7):686–698, 1942.
  - [2] Walter Lang. *Nomarski differential interference-contrast microscopy*. Oberkochen, Carl Zeiss, 1982.
  - [3] Robert Hoffman and Leo Gross. Modulation contrast microscope. *Applied Optics*, 14(5):1169–1176, 1975.
  - [4] Etienne Cuche, Frédéric Bevilacqua, and Christian Depeursinge. Digital holography for quantitative phase-contrast imaging. *Opt. Lett.*, 24(5):291–293, 1999.
  - [5] P. Marquet, B. Rappaz, P. J. Magistretti, E. Cuche, Y. Emery, T. Colomb, and C. Depeursinge. Digital holographic microscopy: a noninvasive contrast imaging technique allowing quantitative visualization of living cells with subwavelength axial accuracy. *Optics Letters*, 30:468–470, March 2005.
  - [6] Pierre Marquet, Christian Depeursinge, and Pierre J Magistretti. Review of quantitative phase-digital holographic microscopy: promising novel imaging technique to resolve neuronal network activity and identify cellular biomarkers of psychiatric disorders. *Neurophotonics*, 1(2):020901–020901, 2014.
  - [7] Euan McLeod and Aydogan Ozcan. Unconventional methods of imaging: computational microscopy and compact implementations. *Reports on Progress in Physics*, 79(7):076001, 2016.
  - [8] Lihong Ma, Gannavarpu Rajshekhar, Ru Wang, Basanta Bhaduri, Shamira Sridharan, Mustafa Mir, Arindam Chakraborty, Rajashekar Iyer, Supriya Prasanth, Larry Millet, et al. Phase correlation imaging of unlabeled cell dynamics. *Scientific Reports*, 6, 2016.
  - [9] Emil Wolf. Three-dimensional structure determination of semi-transparent objects from holographic data. *Optics Communications*, 1(4):153–156, 1969.
  - [10] F. Charrière, A. Marian, F. Montfort, J. Kuehn, T. Colomb, E. Cuche, P. Marquet, and C. Depeursinge. Cell refractive index tomography by digital holographic microscopy. *Optics Letters*, 31(2):178–180, 2006.
  - [11] Olivier Haeberlé, Kamal Belkebir, H Giovaninni, and Anne Sentenac. Tomographic diffractive microscopy: basics, techniques and perspectives. *Journal of Modern Optics*, 57(9):686–699, 2010.
  - [12] Yann Cotte, Fatih Toy, Pascal Jourdain, Nicolas Pavillon, Daniel Boss, Pierre Magistretti, Pierre Marquet, and Christian Depeursinge. Marker-free phase nanoscopy. *Nature Photonics*, 7(2):113–117, 2013.

- [13] Di Jin, Renjie Zhou, Zahid Yaqoob, and Peter TC So. Tomographic phase microscopy: principles and applications in bioimaging. *JOSA B*, 34(5):B64–B77, 2017.
- [14] D. Gabor. A new microscopic principle. *Nature*, 161:777–778, 1948.
- [15] Chanchal bhardwaj and Pradipta Panigrahi. Comparison between digital inline and off-axis holography system for particle field characterization. *13th International Conference on Fiber Optics and Photonics*, page W3A.8, 2016.
- [16] Weijuan Qu, Oi Choo Chee, Yingjie Yu, and Anand Asundi. Recording and reconstruction of digital gabor hologram. *Optik-International Journal for Light and Electron Optics*, 121(23):2179–2184, 2010.
- [17] MH Jericho, HJ Kreuzer, M Kanka, and R Riesenber. Quantitative phase and refractive index measurements with point-source digital in-line holographic microscopy. *Applied Optics*, 51(10):1503–1515, 2012.
- [18] E.N. Leith and J. Upatnieks. Reconstructed wavefronts and communication theory. *JOSA*, 52(10):1123–1128, 1962.
- [19] Etienne Cuhe, Pierre Marquet, and Christian Depeursinge. Spatial filtering for zero-order and twin-image elimination in digital off-axis holography. *Applied Optics*, 39(23):4070, 2000.
- [20] Qu Weijuan, Yu Yingjie, Chee Oi Choo, and Anand Asundi. Digital holographic microscopy with physical phase compensation. *Optics letters*, 34(8):1276–1278, 2009.
- [21] Oleg V Grishin, Ivan V Fedosov, and Valery V Tuchin. Simple technique of fourier-transform holographic microscope with compensation of phase aberration. In *Saratov Fall Meeting 2015*, pages 99171W–99171W. International Society for Optics and Photonics, 2016.
- [22] Eugene Serabyn, Kurt Liewer, Chris Lindensmith, Kent Wallace, and Jay Nadeau. Compact, lensless digital holographic microscope for remote microbiology. *Optics Express*, 24(25):28540–28548, 2016.
- [23] Manon Rostykus and Christophe Moser. Compact lensless off-axis transmission digital holographic microscope. *Opt. Express*, 25(14):16652–16659, Jul 2017.
- [24] Zahra Monemhaghdoost, Frédéric Montfort, Yves Emery, Christian Depeursinge, and Christophe Moser. Dual wavelength full field imaging in low coherence digital holographic microscopy. *Optics express*, 19(24):24005–24022, 2011.
- [25] Youngwoon Choi, Taeseok Daniel Yang, Kyoung Jin Lee, and Wonshik Choi. Full-field and single-shot quantitative phase microscopy using dynamic speckle illumination. *Optics letters*, 36(13):2465–2467, 2011.
- [26] F Dubois and C Yourassowsky. Full off-axis red-green-blue digital holographic microscope with led illumination. *Optics letters*, 37(12):2190–2192, 2012.
- [27] Stefan Witte, Andrius Plauška, Margreet C Ridder, Laura van Berge, Huibert D Mansvelter, and Marie Louise Groot. Short-coherence off-axis holographic phase microscopy of live cell dynamics. *Biomedical optics express*, 3(9):2184–2189, 2012.
- [28] Zahra Monemhaghdoost, Frederic Montfort, Etienne Cuhe, Yves Emery, Christian Depeursinge, and Christophe Moser. Full field vertical scanning in short coherence digital holographic microscope. *Optics express*, 21(10):12643–12650, 2013.
- [29] Tomáš Slabý, Pavel Kolman, Zbyněk Dostál, Martin Antoš, Martin Lošťák, and Radim Chmelník. Off-axis setup taking full advantage of incoherent illumination in coherence-controlled holographic microscope. *Optics Express*, 21(12):14747–14762, 2013.
- [30] Rongli Guo, Fan Wang, Xiaoying Hu, and Wenqian Yang. Off-axis low coherence digital holographic interferometry for quantitative phase imaging with an led. *Journal of Optics*, 2017.
- [31] RN Smartt and WH Steel. Theory and application of point-diffraction interferometers. *Japanese Journal of Applied Physics*, 14(S1):351, 1975.
- [32] H Medeck, E Tejnill, KA Goldberg, and J Bokor. Phase-shifting point diffraction interferometer. *Optics letters*, 21(19):1526–1528, 1996.
- [33] Peng Gao, Baoli Yao, Junwei Min, Rongli Guo, Juanjuan Zheng, Tong Ye, Irina Harder, Vanusch Nercissian, and Klaus Mantel. Parallel two-step phase-shifting point-diffraction interferometry for microscopy based on a pair of cube beamsplitters. *Optics express*, 19(3):1930–1935, 2011.
- [34] Guy Indebetouw and Prapong Klysubun. Space-time digital holography: A three-dimensional microscopic imaging scheme with an arbitrary degree of spatial coherence. *Applied physics letters*, 75(14):2017–2019, 1999.
- [35] Gabriel Popescu, Takahiro Ikeda, Ramachandra R Dasari, and Michael S Feld. Diffraction phase microscopy for quantifying cell structure and dynamics. *Optics letters*, 31(6):775–777, 2006.
- [36] Zhuo Wang, Larry Millet, Mustafa Mir, Huafeng Ding, Sakulsuk Unarunotai, John Rogers, Martha U Gillette, and Gabriel Popescu. Spatial light interference microscopy (slim). *Optics express*, 19(2):1016–1026, 2011.
- [37] Natan T Shaked. Quantitative phase microscopy of biological samples using a portable interferometer. *Optics letters*, 37(11):2016–2018, 2012.
- [38] Pinhas Girshovitz and Natan T Shaked. Compact and portable low-coherence interferometer with off-axis geometry for quantitative phase microscopy and nanoscopy. *Optics express*, 21(5):5701–5714, 2013.
- [39] Yujie Lu, Yunhui Liu, and Tak Kit Lau. Simple, portable, and low-cost microscope based on off-axis digital holography using two spherical waves. *Optics letters*, 39(15):4549–4552, 2014.
- [40] J Kent Wallace, Stephanie Rider, Eugene Serabyn, Jonas Kühn, Kurt Liewer, Jody Deming, Gordon Showalter, Chris Lindensmith, and Jay Nadeau. Robust, compact implementation of an off-axis digital holographic microscope. *Optics express*, 23(13):17367–17378, 2015.
- [41] Jerome Primot. Three-wave lateral shearing interferometer. *Applied optics*, 32(31):6242–6249, 1993.
- [42] Pierre Bon, Guillaume Maucort, Benoit Wattellier, and Serge Monneret. Quadriwave lateral shearing interferometry for quantitative phase microscopy of living cells. *Optics express*, 17(15):13080–13094, 2009.
- [43] Herwig Kogelnik. Coupled wave theory for thick hologram gratings. *Bell System Technical Journal*, 48(9):2909–2947, 1969.
- [44] Jacques E Ludman. Approximate bandwidth and diffraction efficiency in thick holograms. *American Journal of Physics*, 50(3):244–246, 1982.
- [45] Oleg M Efimov, Leonid B Glebov, Larissa N Glebova, Kathleen C Richardson, and Vadim I Smirnov. High-efficiency bragg gratings in photothermorefractive glass. *Applied optics*, 38(4):619–627, 1999.
- [46] Zahra Monemhaghdoost, Frédéric Montfort, Yves



- Emery, Christian Depeursinge, and Christophe Moser. Off-axis digital holographic camera for quantitative phase microscopy. *Biomedical optics express*, 5(6):1721–1730, 2014.
- [47] Joseph W Goodman. *Introduction to Fourier optics*. Roberts and Company Publishers, 2005.
- [48] G. Indebetouw and P. Klysubun. Spatiotemporal digital microholography. *Optical Society of America Journal A*, 18:319–325, February 2001.
- [49] Prapong Klysubun and Guy Indebetouw. A posteriori processing of spatiotemporal digital microholograms. *JOSA A*, 18(2):326–331, 2001.
- [50] Jisoo Hong and Myung K Kim. Single-shot self-interference incoherent digital holography using off-axis configuration. *Optics letters*, 38(23):5196–5199, 2013.
- [51] Joseph Rosen and Gary Brooker. Digital spatially incoherent fresnel holography. *Optics letters*, 32(8):912–914, 2007.
- [52] Dinesh N Naik, Giancarlo Pedrini, Mitsuo Takeda, and Wolfgang Osten. Spectrally resolved incoherent holography: 3d spatial and spectral imaging using a mach-zehnder radial-shearing interferometer. *Optics letters*, 39(7):1857–1860, 2014.
- [53] Dilband Muhammad, Cuong M Nguyen, Jihoon Lee, and Hyuk-Sang Kwon. Spatially incoherent off-axis fourier holography without using spatial light modulator (slm). *Optics Express*, 24(19):22097–22103, 2016.
- [54] Igor V Ciapurin, Leonid B Glebov, and Vadim I Smirnov. Modeling of phase volume diffractive gratings, part 1: transmitting sinusoidal uniform gratings. *Optical Engineering*, 45(1):015802–015802, 2006.
- [55] A.E. Siegman. The antenna properties of optical heterodyne receivers. *Applied Optics*, 5(10):1588, 1966.
- [56] J. W. Goodman and R. W. Lawrence. digital formation of images from electronically detected holograms. *Applied Physics Letters*, 11(3):77–79, 1967.
- [57] U. Schnars and W. Juptner. Direct recording of holograms by a ccd target and numerical reconstruction. *Appl. Opt.*, 33:179–181, 1994.
- [58] U. Schnars and W. P. O. Juptner. Digital recording and numerical reconstruction of holograms. *Meas. Sci. Technol.*, 13:R85–R101, 2002.
- [59] Myung K Kim, Lingfeng Yu, and Christopher J Mann. Interference techniques in digital holography. *Journal of Optics A: Pure and Applied Optics*, 8(7):S518–S523, 2006.
- [60] Pascal Picart and Julien Leval. General theoretical formulation of image formation in digital fresnel holography. *JOSA A*, 25(7):1744–1761, 2008.
- [61] Nicolas Verrier and Michael Atlan. Off-axis digital hologram reconstruction: some practical considerations. *Appl. Opt.*, 50(34):H136–H146, Dec 2011.
- [62] Pablo Piedrahita-Quintero, Raul Castañeda, and Jorge Garcia-Sucerquia. Numerical wave propagation in imagej. *Applied optics*, 54(21):6410–6415, 2015.
- [63] Tatiana Latychevskaia and Hans-Werner Fink. Practical algorithms for simulation and reconstruction of digital in-line holograms. *Applied optics*, 54(9):2424–2434, 2015.
- [64] <http://holovibes.com>.
- [65] Carlos Trujillo, Raúl Castañeda, Pablo Piedrahita-Quintero, and Jorge Garcia-Sucerquia. Automatic full compensation of quantitative phase imaging in off-axis digital holographic microscopy. *Applied optics*, 55(36):10299–10306, 2016.
- [66] HJ Kreuzer, MJ Jericho, IA Meinertzhagen, and W. Xu. Digital in-line holography with photons and electrons. *Journal of Physics: Condensed Matter*, 13(47):10729–10741, 2001.
- [67] Daniel Ott, Marc SeGall, Ivan Divliansky, George Venus, and Leonid Glebov. High-contrast filtering by multipass diffraction between paired volume bragg gratings. *Applied optics*, 54(31):9065–9070, 2015.